Understanding the damage mechanisms in 3D layer-to-layer woven composites from thermal and acoustic measurements

Libor Navrátil, Vincent Le Saux, Yann Marco, Zoheir Aboura, Walid Harizi, Clément Cuniberti, Nicolas Carrere, Sylvain Leclercq

Journal Title
XX(X):1–18

DOI: 10.1177/ToBeAssigned
www.sagepub.com/
SAGE

Understanding the damage mechanisms in 3D layer-to-layer woven composites from thermal and acoustic measurements

L. Navrátil[1,3], V. Le Saux[1], Y. Marco[1], Z. Aboura[2], W. Harizi[2], C. Cuniberti[2], N. Carrere[1], S. Leclercq[3]

Abstract

This article deals with an interlock woven composite and aims at providing a better understanding of the dissipative mechanisms activated under cyclic loadings and describing the damage scenario characteristic of heat build-up experiments. Since the ultimate objective of heat build-up experiment analyses is usually fatigue life predictions that are based on constitutive modelling, the correct interpretation of experimental results is essential. Three different loading protocols are proposed. The instrumentation of these experiments includes infrared thermometry and acoustic emission monitoring. The results show that the coupling of these two techniques provides useful information in order to identify the most important dissipation sources: viscoelasticity, damage and friction. Furthermore, by analysing different loading sequences, it is possible to elaborate the dissipation evolution scenario as well as the damage evolution scenario occurring during heat build-up experiments.

Keywords

3D woven composite, infrared thermography, acoustic emission, cyclic loading

Introduction

Research context

The broad implementation of composite materials is the result of their excellent specific strength and stiffness properties. Polymer matrix woven or textile composites have been gaining popularity since they lack the drawbacks found in commonly used laminated composites: low damage resistance and poor out-of-plane properties[1–9]. Since many of the industrial applications undergo cyclic loadings that can lead to fatigue failure, the characterisation of the fatigue properties of the material has proved to be crucial in order to ensure the reliability of the structure[10]. However, fatigue campaigns are usually costly due to the long duration of mechanical tests, as well as the high number of specimens that require testing before experimental scattering can be taken into account. That is why, over the past years, efforts have been made to accelerate this characterisation process.

One of the approaches is based on the analysis of the heat build-up response under cyclic loadings. Since the early studies that focussed mostly on metallic materials[11–13], this technique has been tested and adapted to other materials

[1]ENSTA Bretagne, Institut de Recherche Dupuy de Lôme (iRDL), UMR CNRS 6027
[2]Université de Technologie de Compiègne, Roberval (Mechanics, Energy and Electricity)
[3]Safran Landing Systems

Corresponding author:
Vincent Le Saux, ENSTA Bretagne, Institut de Recherche Dupuy de Lôme (iRDL), UMR CNRS 6027
Email: vincent.le_saux@ensta-bretagne.fr

such as elastomers [14,15], or short fibre composites [16–19]. Most approaches aim at evaluating the dissipated energy based on temperature variations. This dissipated energy is then plotted against the stress (or strain) amplitude leading to the so-called heat build-up curve. The following step is to analyse this curve in order to obtain the endurance limit [20], the mean S-N curve (the curve that plots the stress amplitude against the number of cycles to failure, also known as a Wöhler curve) [15,19,21] or, even the S-N curve with the associated scattering [13,22].

Yet, the accuracy of these fatigue life predictions is determined by the the complexity of the dissipating mechanisms involved that govern fatigue failure and their accurate modelling. While the endurance limit can be obtained using an empirical analysis of the change in slope of the heat build-up curve, in order to predict the S-N curve with the associated scatter, it is necessary to relate the dissipative energy to damage mechanisms through a constitutive modelling introducing a probabilistic failure criterion. However, the use of this approach remains limited in the case of woven composites. The first difficulty is the lack of information about the temperature distribution inside the specimen as the instrumentation which is commonly used (an infrared camera at best) gives access only to the surface temperature fields. The second difficulty lies in the constitutive modelling that is complicated mostly due to a large number of dissipative mechanisms, which can include viscoelasticity, plasticity and damage.

The damage scenario of woven composites is particularly complex due to the composite microstructure and involves several phenomena: matrix cracking, inter-yarn and intra-yarn cracking, inter-ply and intra-ply delamination [7,23–27]. The description of the damage process can rely on the use of several non-destructive testing and evaluation (NDT&E) techniques. One of the commonly used techniques to locate the cracks is the acoustic emission (AE) method. AE is historically seen as one of the most effective NDT&E methods to evaluate mechanical damage in polymer-matrix composite (PMC) materials. It is defined as an energy release phenomenon in the form of transient elastic waves resulting from some local micro-displacements internal to a material subjected to a stress [28]. The elastic waves emitted (acoustic signals or hits) are initially ultrasonic volume waves (longitudinal or transverse), but undergo mode conversions, depending on the geometry of the tested structure, which transform into Lamb waves. The AE method consists in detecting these signals in order to extract real-time information on the material damage [29].

The bibliography is very abundant regarding the use of the AE technique for the damage characterisation of PMCs. The synthesis of these works into chronological order separates analysis of the data processing mode into two parts: single parameter or multi-parameter analysis. [30]. Conventional single-parameter processing of AE data considers a single descriptor among several to describe an acoustic signature corresponding to a specific damage mechanism [30–35]. The parameters that can be used are numerous (amplitude, duration, rise time, counts, frequency, energy, etc.) and can be extracted directly from the temporal signal or its frequency spectrum. Most single-parameter studies use amplitude as a discriminating descriptor of the damage mechanisms. The amplitude describing the acoustic signatures varies from one test to another and from one study to another depending on the material studied, the sensors used, their coupling method, the system, the threshold acquisition, etc. Therefore, it is very difficult to make a comparison between all these studies. Likewise, a single damage mechanism, such as matrix cracking, can produce a wide range of amplitudes. Thus, several studies [33,34] present some overlapping intervals for two damage mechanisms, which does not allow the AE amplitude and a particular damage mode to be correlated with any certainty. To overcome these problems, multivariable or multiparameter analysis is employed.

The authors attempted to analyse several AE descriptor signals using many different classification algorithms. A supervised classification requires prior knowledge of the number of classes (damage mechanisms). On the other hand, an unsupervised classification is chosen in the case where the classes are not known a priori by the user. It is thus interesting to opt for the unsupervised approach and consider that the operator does not have any information beforehand on the number of classes or damage mechanisms existing in the material studied. The most used unsupervised classifier for the discrimination between the

damage mechanisms of PMCs is the K-means. It is one of the classification algorithms with ”mobile centres”, and it is widely used due to its simplicity of implementation. K-means is an iterative method of partitioning data by the concept of minimising intra-group variance[30]. The coordinates of the group centres are initialised randomly or manually. Then, each input vector (acoustic hit) is assigned to the nearest group, depending on the Euclidean distance between the input entity and the group centres. Then, by randomly changing the coordinates of the centres, the procedure is repeated until no change in the coordinates of the centres is reported, and at this stage, the algorithm converges[36].

Other techniques that can provide information on the evolution of the damage process are: optical microscopy, scanning electron microscope (SEM) technology[37], X-ray computed tomography (CT)[5] or Synchrotron radiation computer tomography (SRCT)[38]. These experimental methods can provide information on the number and the geometry of the cracks and voids. However, the evaluation of their contribution to the energy dissipation remains limited.

Article objectives

This work examines an interlock woven composite material. The main objective is to develop a better understanding of the dissipative mechanisms activated under cyclic loadings applied during a heat build-up test in order to pave the way for fatigue life predictions based on constitutive modelling. Yet, this is clearly not an easy task because the dissipation mechanisms are numerous, and, furthermore, the damage induced in the material introduces interfaces at different scales that can generate friction as an additional dissipation source. This element represents the first original aspect of this work as the studies conducted on this family of materials did not seek to identify the underlying mechanisms but rather settled for an empirical analysis of the heat build-up curve[6,39].

This study mostly relies on the use of two techniques. The first is infrared thermometry that gives access to temperature fields on a sample’s surface. The second technique is acoustic emission that monitors the occurrence of cracks over the full volume of the sample. In order to obtain the experimental database required, two sets of experiments were carried out. The first focussed on obtaining reliable data which were suitable for the subsequent post-processing. This post-processing consists in the generation of dissipation and thermo-elastic coupling fields[19] and the specific thermal image processing method developed for this study. The first method seeks to detect thermal events linked to the appearance of cracks. The second method, used when cracks have been induced in the material, is designed to highlight the areas with a high intensity of friction generated by the relative movements between crack faces. In order to remain concise, only a brief summary of these two original techniques will be given in this article and their full description is detailed in[40]. The second set of experiments simultaneously uses infrared imaging and acoustic emission monitoring, which allows the correlation of the thermal and the acoustic signatures and provides the experimental results required for the description of the damage progress, as conducted in[41]. The use of this experimental set-up constitutes the second main original aspect of this study as the coupling of infrared imaging and acoustic emission monitoring has not yet been used during heat build-up experiments for these materials.

In the following, the first section presents the material, the samples’ geometry and illustrates the loading protocols. The second section describes the thermal characterisation specifying the post-processing techniques developed during this study. The third section includes the description via acoustic emission monitoring. The fourth section details the experimental results, and, finally, the fifth section analyses the results and proposes a dissipation evolution scenario associated to the heat build-up tests. The role of different dissipative mechanisms is analysed, their contributions to the total dissipated energy are evaluated as well as the evolution of their contributions with respect to the applied stress.

Experimental settings

Material and samples

This study focusses on a woven composite material produced for research purposes by the Safran Group. This woven composite is an unbalanced 3D layer-to-layer interlock consisting of 48k carbon fibre yarns consolidated with an epoxy resin. The material contains 8 plies yielding a total thickness of 7.5 mm. Dimensions of the 3D woven pattern along the direction of the warp yarns and the direction of the weft yarns are comprised within the interval from 20 to 40 mm. The yarn sections are of a millimetre size. The overall fibre volume fraction is equal to approximately 0.6. The intra-yarn fibre volume fractions are equal to 0.8 and 0.88 for the yarns in the warp and weft direction respectively.

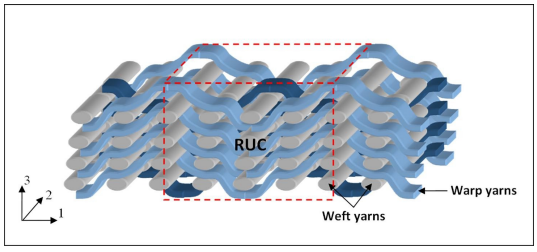

Figure 1. Illustration of a typical woven composite architecture[42].

Figure 2 presents the geometry and dimensions of the coupons used in this study.

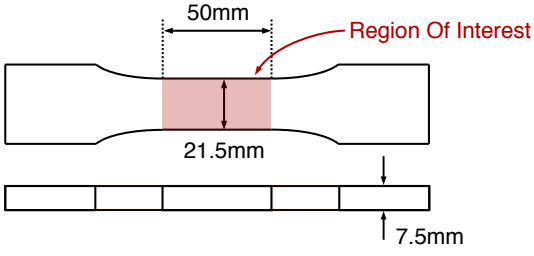

Figure 2. Specimen geometry.

These coupons were machined out of composite panels produced by the resin transfer moulding process, the specimen axis being parallel to the weft direction. Due to the considerable size of the weaving pattern, the specimen shape is a non-standard one[43].

Loading protocol

The experiments were performed using two Instron servo-hydraulic testing machines of 100kN and 250kN capacities. Three different loading protocols were used during the campaign, each protocol applying a set of loading steps during which the stress amplitude was held constant (Figure 3). For the sake of clarity, stress henceforth refers to the average applied stress, as the real stress distribution is heterogeneous due to the complex microstructure of the material.

The stress ratio is equal to $R_\sigma = 0.05$. Another campaign applying a load ratio of $R_\sigma = -1$ was carried out as well. The results are available in[40].

Heat build-up protocol The heat build-up protocol consists in applying a sequence of loading steps of increasing stress amplitude, the stress amplitude remaining constant for each step. This type of protocol is classic in the literature[14,19,21] and its objective is to illustrate the relation between the dissipated energy and the applied stress amplitude defined as $\sigma_{amp} = (\sigma_{max} - \sigma_{min})/2$.

Reverse heat build-up protocol The reverse heat build-up protocol uses a sequence of loading steps of decreasing stress amplitude. This practice aims at highlighting the subsequent effect of an overload on the values of the dissipated energy for lower stress amplitudes.

Gradual heat build-up protocol The gradual heat build-up protocol uses a sequence of loading steps of increasing and decreasing stress amplitude enabling a more continuous description of the loading history effect. The reverse heat build-up protocol and the gradual heat build-up protocol have not been described up to now in the literature, to the authors' knowledge.

It should be added that the maximum loading step applied during each experiment should lead to a maximum stress corresponding to approximately 50-70% of the ultimate strength of the material. Uniformly distributed loading steps in this range should bring to light a representative signature of the the dissipative mechanisms occurring under cyclic loadings.

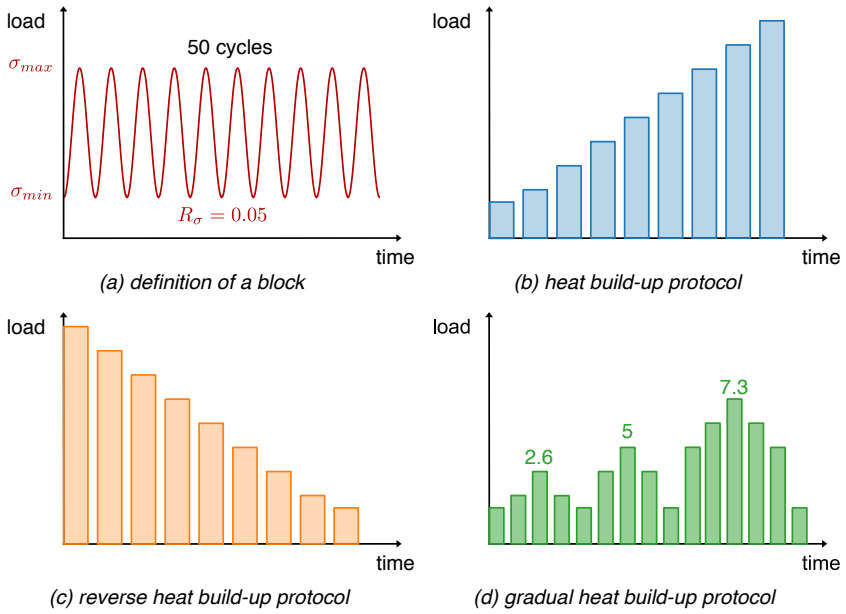

(a) definition of a block (b) heat build-up protocol (c) reverse heat build-up protocol (d) gradual heat build-up protocol

Figure 3. Loading protocols.

Temperature field analyses

Although temperature is already a valuable indicator, it is not an intrinsic characteristic of the material. It is, therefore, necessary to retrieve the heat sources responsible for these temperature variations. This section gives information on the methods used to obtain these data.

Dissipated energy and thermoelastic coupling field evaluation The approach based on adiabatic analysis and presented in former publications [15,18,21,44] was selected for this study since not only does it give access to the mean values, but it also enables the evaluation of the dissipated energy and thermoelastic coupling fields. Moreover, a reduced amount of cycles limits damage accumulation during the experiment. Thus, temperature investigations focus on the first loading cycles of each loading step, explaining why the number of cycles applied in one loading sequence is limited to 50 (Section *Loading protocol*). The determination of dissipated energy fields requires the heat equation to be resolved [15,45] :

$$\rho c_p \frac{\partial T}{\partial t} + div(\vec{q}) = \Delta + r + \mathcal{C}_e + \mathcal{C}_t \qquad (1)$$

with T the temperature, $\vec{q}$ the heat flux, Δ the dissipation, r the external heat supply, $\mathcal{C}_e$ the contribution of the thermoelastic coupling and $\mathcal{C}_t$ the thermomechanical coupling. The material parameters involved in the equation are the specific mass ρ and the specific heat c_p.

The previous equation can be simplified using several hypotheses. The most important of these hypotheses are presented in this paragraph and the reader is referred to previous publications [15,18,19,21] for an exhaustive description of all the underlying assumptions. First, the temperature variations are considered to be small enough to consider the material parameters constant and to neglect the dependency of the thermomechanical coupling to the temperature. Considering the temperature variation θ (difference between the instantaneous and initial temperature, $T - T_0$) rather than the temperature T allows for compensating the external heat supply r that is assumed constant in time. Furthermore, an average evaluation of the dissipation is done over a mechanical cycle allowing to replace the instantaneous dissipation term Δ with the cyclic dissipated energy $\Delta^\star$ that is independent of the mechanical frequency f_r. Finally, the simplified form of the heat equation can finally be written as follows:

$$\rho c_p \frac{\partial \theta}{\partial t} = f_r \Delta^\star + \mathcal{C}_e \qquad (2)$$

As stated in Leveuf *et al.*[19], this equation is local, it is, therefore, convenient to transpose the temperature fields measured into the reference configuration prior to analysis. As a matter of fact, one pixel does not correspond to one material point since the sample deforms under the applied loading, whereas the camera is fixed. This motion therefore needs to be compensated otherwise the precision might be reduced. This is especially true in the case of woven composites as the complex microstructure leads to heterogeneous heat source fields. The compensation is done systematically via a routine developed in-house that analyses the displacements of two high emissivity markers located outside the region of interest (ROI). This allows compensation for the translation motion of the ROI as well as the average dilatation (contraction) of its original height (width)[40].

The pixelwise post-processing of the temperature fields enables access to the dissipated fields used in this study. The identification is based on the following equation[19]:

$$\theta(t) = \frac{f_r}{\rho c_p}\Delta^* \cdot t + C_e \sin(f_r \cdot t + \varphi) \qquad (3)$$

where φ represents the phase lag between the mechanical loading and the temperature signal. The global mechanical hysteresis was observed to stabilise after 4 cycles. Thus, in order to respect the constant cyclic dissipation hypothesis, the lower bound of the identification interval must not be inferior to 2 seconds (as the loading frequency was set to 2 Hz). The duration of the identification interval was set to 4 seconds (Figure 4).

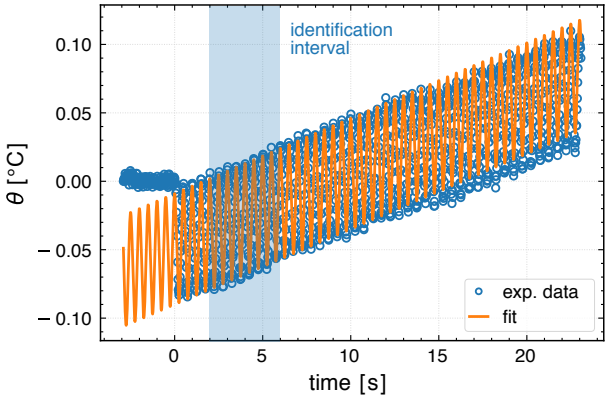

Figure 4. Illustration of the identification interval.

The characteristic time of the specimen was evaluated, using the mean cooling curve[46] to be approximately 300 s (Figure 5). It is, therefore, reasonable to assume

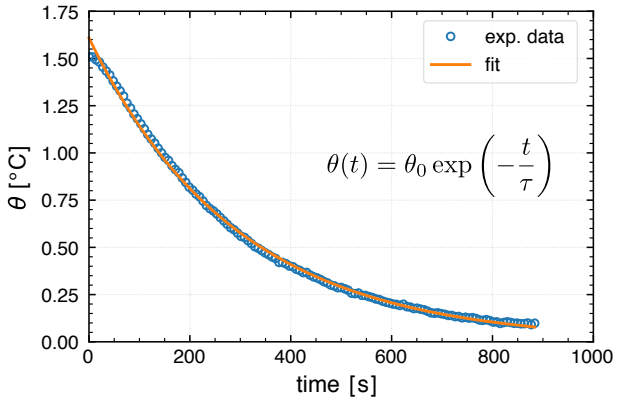

Figure 5. Evaluation of the characteristic time.

that the adiabatic condition was globally satisfied. The heat build-up curve was then obtained by plotting the average values of the dissipated energy fields against the stress amplitude (Figure 6-(a))[19]. The mean value of the dissipated energy is computed over the region of interested and plotted against the loading stress amplitude applied in the respective loading step. The thermoelastic coupling curve was also obtained in a similar way, as illustrated in Figure 6-(b). It should be mentioned that a

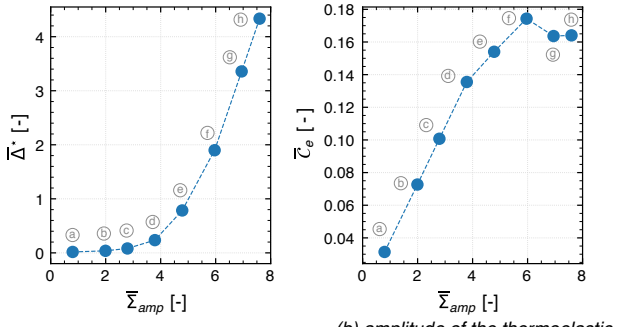

(a) heat build-up curve

(b) amplitude of the thermoelastic coupling contribution

Figure 6. Examples of heat build-up and thermoelastic coupling contribution curves.

direct interpretation of the thermoelastic coupling values is quite complex since the relation between the thermoelastic coupling contribution and local stress components would require advanced constitute modelling, based upon a fine description of the microstructure. Considering this, no quantitative analyses are presented in this article as a

comparison between different tests could be misleading. Nevertheless, the thermoelastic coupling evolution obtained for a gradual heat build-up test will be presented in Section *Gradual heat build-up test* and discussed in Section *Gradual heat build-up results*. As all measurements were performed on the same sample, the microstructure pattern was the same for the whole test.

Thermal event detection When analysing the infrared films recorded during the tests, it is possible to observe certain local irregularities that occur during the loading period. These irregularities will henceforth be called *thermal events*. One of these events is illustrated in Figure 7.

These thermal events included a steep increase in temperature variation, however, the area affected by this temperature increase remained relatively small. The duration of these events was limited to a few milliseconds. Then, the temperature increase was diffused, and the affected zone returned to a dynamic thermal equilibrium. Figure 7 also illustrates that the occurrence of the thermal event induced a decrease in the amplitude of the temperature oscillations. This reduction results from a decrease in the thermo-elastic coupling contribution. This phenomenon was explained thanks to posterior surface observations that revealed that thermal events are linked to the creation of cracks[40].

The analysis of these events required a dedicated detection protocol due to their local nature as well as their abrupt duration. In order to highlight the regions associated with thermal events, a thresholding routine was adopted. The core of this routine consists in identifying all the pixels exhibiting a temperature increase of more than 0.3°C between two successive images (this corresponds to a time difference of 0.02 s). The identified pixels were plotted in the form of binary maps as illustrated in Figure 8. The value of the threshold was fixed based on sensitivity studies and the results of meso-scale cooling observations (not presented in this article, refer to[40]). The maps display the thermal events detected during each loading sequence of one heat-build up test. By analysing these results, it is possible to compute the number of thermal events that occurred during each sequence and the relative surface (compared to the full surface observed) affected by these events. The evolutions of these two characteristics are discussed in Section *Heat build-up test result*.

Frequency analyses In order to better understand the thermomechanical behaviour of the material, the pixelwise post-processing routine described in[19] was extended to the frequency analyses[47–49]. By interpreting the temperature evolution of a pixel as a signal, it is possible to transform this signal into the frequency domain using the Discrete Fourier Transform and plot its amplitude spectrum. When working in the frequency domain, it is possible to retrieve the amplitudes that correspond to specific frequencies and plot the results in the form of amplitude fields. The amplitude fields corresponding to double the loading frequencies are of a particular importance as they could highlight the regions with high intensity of friction[40]. As mentioned in the introduction, this phenomenon can be observed only under relatively high stresses when cracks have been induced in the material since friction can only be generated by the relative movement of crack faces. When the specimen is loaded, the local deformation field in the vicinity of a crack may press the crack faces into contact and move them against each other. The unloading phase will, thus, inevitably result in a relative movement in the opposite direction. The friction, and thus heat dissipation caused by these displacements generate measurable temperature increases. Since these temperature variations accompany the loading as well as the unloading period of each loading cycle, it is reasonable to assume that their predominant amplitude is that which varies at double the loading frequency.

Acoustic emission monitoring

As mentioned earlier, the objective in using acoustic emission monitoring is to provide the information necessary to describe the damage scenario. Indeed, when the material is stressed according to the different loading protocols cited in Section *Loading protocol*, it releases deformation energy in the form of transient elastic waves that propagate inside the material until reaching the acoustic sensors coupled on the surface of the test specimens. Thus, all AE hits are recorded in real-time.

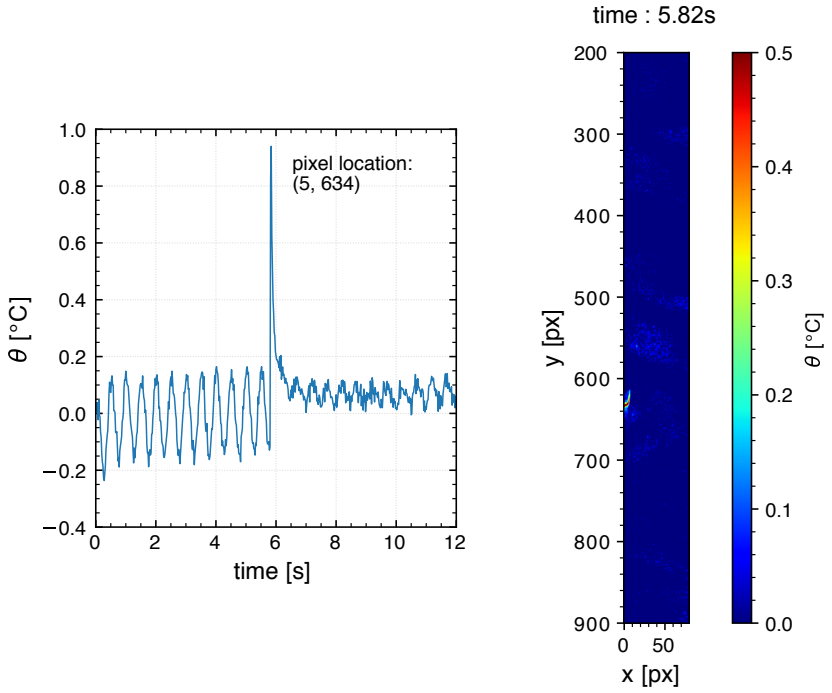

(a) evolution of the temperature of a pixel during the test

(b) temperature variation map for a specific frame

Figure 7. Illustration of a thermal event.

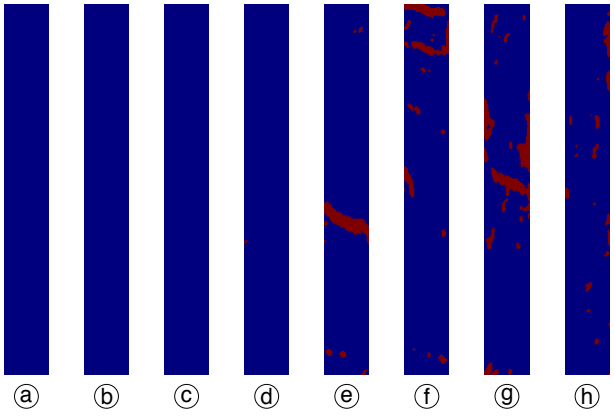

Figure 8. Illustration of the thermal events detected during different loading steps.

Acoustic emission processing

In our case, the AE data can be represented by a matrix X of $n \times 13$ dimensions, n is the number of hits. There are thirteen variables (or descriptors) describing the n recorded hits during an AE test. These variables defined in the Physical Acoustics Corporation manual[50] are: rise time, counts to peak, counts, duration, amplitude, energy, absolute energy, average frequency, ASL (Average Signal Level), RMS (Root Mean Square), reverberation frequency, initiation frequency and signal strength. It should be noted that the number n depends on the type of the sample tested and its acoustic emissivity. Thus, each AE hit is a vector x_i^j ($i = 1, n$ and $j = 1, 13$) made up of 13 components.

The $K-$means algorithm is an iterative method of partitioning acoustic data by the concept of minimising intra-class variance. The coordinates of the class centres C_I^j ($I = 1, K$ with K the number of classes and $j = 1, 13$) are initialised randomly or manually. Then, each input vector x_i^j is assigned to the nearest group, depending on the Euclidean distance (Equation 4) between the input entity x_i^j and the centres C_I^j.

$$d(x_1^j, C_I^j) = \sqrt{\sum_{j=1}^{13} \left(x_1^j - C_I^j\right)^2} \tag{4}$$

The number of classes K minimising the Davies and Bouldin (DB) criterion is defined by Equation 5 where d_i and d_j are the averages of the Euclidean distances within

the class of groups i and j, respectively. D_{ij} is the distance between the centre of the two groups i and j.

$$DB = \frac{1}{k}\sum_{i=1}^{k}\max_{i\neq j}\left(\frac{d_i + d_j}{D_{ij}}\right) \quad (5)$$

During this study, the number of classes K was evaluated by applying the DB criterion on the acoustic dataset recorded during each mechanical loading based on the three proposed protocols. Similarly, since the main objective of this study is the evaluation of the dissipated energy variation, each acoustic class was described by two pertinent descriptors: the event counts and their absolute energy.

Experimental set-up

The experimental set-up is illustrated in Figure 9. A

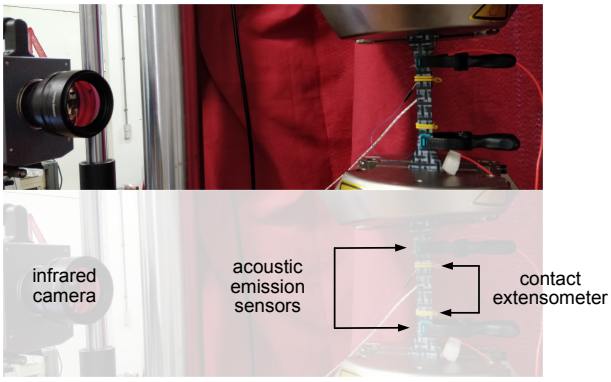

Figure 9. Illustration of the experimental set-up for combined IR and AE measurements.

mechanical extensometer with a gauge length of 10 mm attached to the specimen surface was used to monitor the nominal average strain. The nominal average stress was calculated from the measured force divided by the initial cross-sectional area. These two variables (stress and strain) were used for the calculation of the elastic modulus measured at the beginning of a loading cycle, as mentioned in Section *Acoustic emission monitoring*. Two AE transducers (Micro-80, from the Physical Acoustics Corporation) with a 40 dB pre-amplification were coupled outside the observation area (ROI) with silicone grease on the same face of the samples at a distance of 80 mm between their centres, symmetrically arranged about the centre of the length of the specimen. The simultaneous use of two sensors enabled the signals to be located and allowed those coming from outside the region of interest to be removed. The infrared camera was focussed on the side face during the entire campaign. It should be mentioned that the quality of the temperature measurements, as well as the size of the measured temperature fields, was reduced due to the presence of the extensometer and the AE sensors. However, these perturbations were not problematic since the goal was to verify the consistency with respect to the previously obtained infrared results. Figure 10 compares the respective heat build-up curves obtained and illustrates that this consistency was, indeed, verified.

Results

Heat build-up test results

Infrared imaging results Figure 10 summarises the results obtained for four different specimens. As Figure 10 indicates, the temperature measurements were carried out both on a side face as well as on a front face. The good

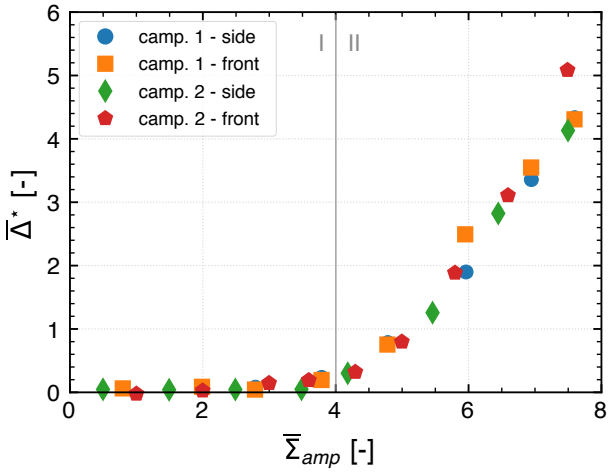

Figure 10. Illustration of the experimental scattering between two different campaigns carried from both the front and side face.

consistency of the results pleads for the dissipated energy to be considered as a representative macroscopic feature of the sample, over the evaluated volume. Furthermore, the side face observations were obtained for two different loading sequences, which illustrates that the loading sequence did not influence the dissipated energy measured in this case.

As evoked earlier, it is apparent that the experimental set-up, including a mechanical extensometer and acoustic emission sensors, does not affect the average value of the dissipated energy as the respective heat build-up curve correlates well with the formerly obtained results (campaign 1 vs. campaign 2).

Figure 11 shows a typical evolution of the number of thermal events detected during a heat build-up test as well as the evolution of their associated surface. An obvious increase in event count occurs when the maximum stress amplitude exceeds the value of 4 MPa/MPa. Furthermore, it is apparent that the intensity of the formation of thermal events culminates for 7 MPa/MPa and then decreases steeply during the last loading sequence.

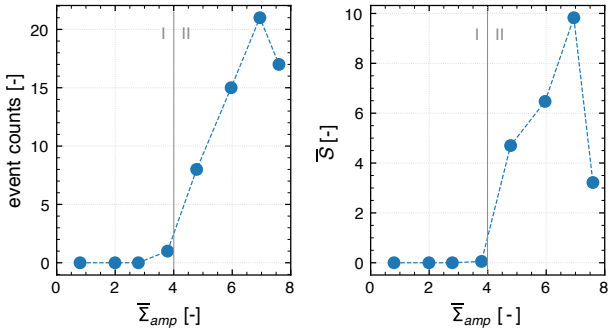

Figure 11. Typical evolution of the thermal event detection results during a heat build-up test.

Acoustic emission monitoring Figure 12 illustrates the evolution of the tangent elastic modulus measured during the 2^{nd} and 49^{th} cycle of each loading step, evaluated during the beginning of the loading part of the cycle thanks to the extensometer. The first significant loss of stiffness occurs during the 6^{th} loading step under the amplitude of 5 MPa/MPa.

The DB criterion (Equation 5) is applied to the acoustic emission dataset. It turns out that the number of classes K minimizing the DB criterion is equal to 3. Thus, the K-means method using the calculation of the Euclidean distance (Equation 4) is applied on the recorded AE hits with a number of classes equal to 3. Labelling these three classes was a fairly easy task since the thickness of the composite specimens was inspected in real-time by in-situ video-microscope. Three classes have been identified:

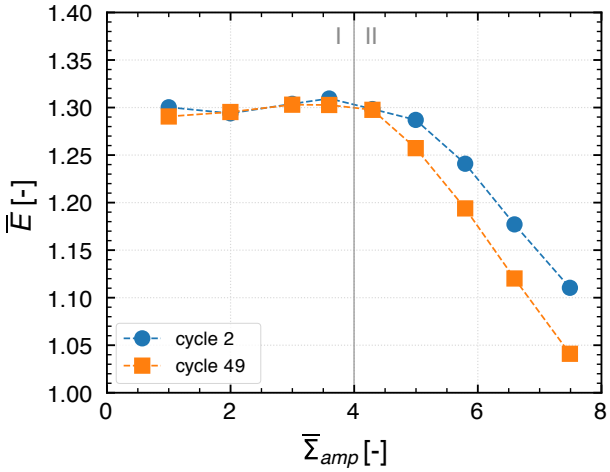

Figure 12. Evolution of the elastic modulus evaluated during a heat build-up test.

major cracks, debonding or matrix cracks and microcracks (or minor cracks with very small size).

Figure 13 summarises the evolutions of the event counts and the normalised acoustic energy for each class identified. One can observe that below 4 MPa/MPa, all classes present low acoustic emission activity and, then, exhibit a sharp increase in terms of both, event count and the acoustic energy. Then, it is possible to observe that, for all types of events, the total number of events as well as the acoustic energy culminate for a stress amplitude of 5-6 MPa/MPa with a slight rebound of the major crack family noticeable during the last sequence. Furthermore, the analysis of the acoustic events did not show any trend or correlation concerning the 1D position that is measured along the specimen axis.

Reverse heat build-up test

Infrared imaging results Figure 14-(a) compares the results of a reverse heat build-up test (schematically presented in Figure 3c) with the results of the heat build-up experiments presented in the previous section. It is important to note that all the thermal events detected during this experiment occurred during the first loading sequence (under the highest stress), as illustrated in Figure 14-(b). For the same stress amplitude, the first step of the reverse test seems to induce more damage than the last step of a classic heat build-up test. This could be explained

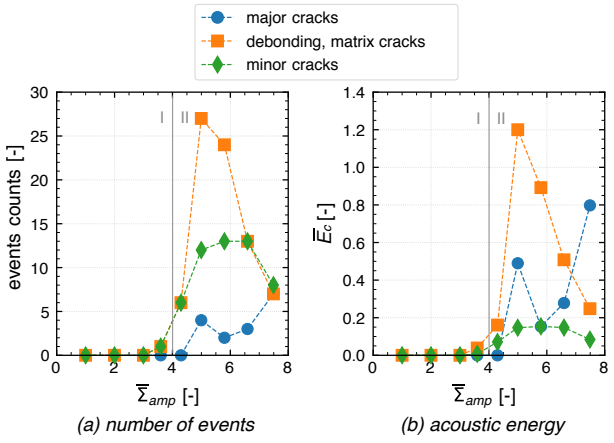

(a) number of events (b) acoustic energy

Figure 13. Evolution of the material acoustic activity during a heat build-up test.

by the progressive amplitude increase during the classic protocol that leads to quite gradual damage evolution. The comparison between Figure 14-(c) and Figure 14-(d) reveals that the peaks of the energy dissipation correspond quite closely to those revealed by the $2 \times f$ analysis and identified as related to friction.

Acoustic emission monitoring This section presents the acoustic emission monitoring results obtained during the reverse heat build-up test. As illustrated in the previous section, it is obvious that the most severe damage occurs during the first loading step (Figure 15). Indeed, all the major crack events, that are the most critical in terms of damage, were detected during the first loading step and even though the micro-cracking continued to develop during the following loading steps, its overall impact remained limited in terms of the acoustic energy (Figure 15-(b)).

Gradual heat build-up test

This section presents the gradual heat build-up test results. The loading protocol is schematically illustrated in Figure 3. Figure 16-(a) presents the evolution of the global thermoelastic coupling curve. It is apparent that while the loading amplitude remains inferior to 3.4 MPa/MPa, this evolution stays linear and the slope remains the same for loading and unloading sequences. As the stress amplitude increases further and exceeds 3.4 MPa/MPa, a change of slope becomes visible. Then, the unloading and reloading phase exhibit a common linear curve, with a reduced slope compared to the initial one. Again, when the maximum stress amplitude has been reached, a change of slope occurs. The last unloading sequence exhibits a linear behavior, with a reduced slope with respect to the two previous unloading sequences.

Figure 16-(b) superposes the experimental results with the heat build-up results presented in Section *Heat build-up test results*. It is apparent that the gradual heat build-up envelope coincides with the results of the heat build-up experiments. Furthermore, it is obvious that the value of the evaluated dissipated energy is history dependent, which is graphically expressed by the curve hysteresis (differences between the loading and unloading curves).

Figure 17 illustrates the results of the first loading sequence with its stress amplitudes remaining inferior to 3 MPa/MPa. As illustrated in Figure 17, only one thermal event was detected during the third loading step. This thermal event reflects probably the creation of a microcrack in the resin-rich area situated in the left of the micrography shown in Figure 17-(c). Nevertheless this thermal event did not affect the value of the total dissipated energy as the curve does not show any sign of hysteresis. The small difference between the values obtained for the two 1 MPa/MPa steps can be explained by the precision of the temperature measurements, as the temperature variations are particularly low in this loading range.

Figure 18 illustrates the results of the second loading sequence of the gradual heat build-up protocol. The maximum stress amplitude applied during this sequence was equal to 5 MPa/MPa. Figure 18-(a) displays all the thermal events detected up to this stress level (and hence during the whole loading sequence since the last five loading steps do not introduce new cracks into the specimen). Figures 18-(b) and 18-(c) present the dissipated energy and the $2 \times f$ amplitude maps obtained during the first 3.4 MPa/MPa loading step. Figures 18-(d) and 18-(e) present these maps obtained for the equivalent loading steps observed during the unloading part of the sequence. Whereas the increase in dissipated energy between these two steps is evident and seems to correlate with the previously detected thermal events, the $2 \times f$ amplitude values remain negligible in both cases.

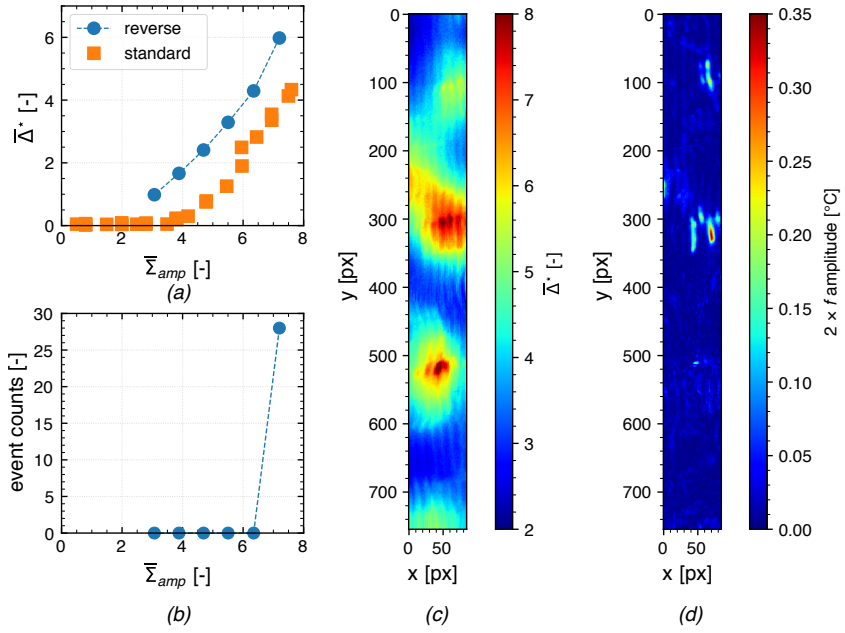

Figure 14. Infrared imaging results of the reverse heat build-up test : (a) dissipation curve, (b) number of thermal events counted during the reverse heat build-up test, (c) dissipation mapping for the normalised stress amplitude $\overline{\Sigma}_{amp} = 6.3$ and (d) $2 \times f$ amplitude mapping for the normalised stress amplitude $\overline{\Sigma}_{amp} = 6.3$.

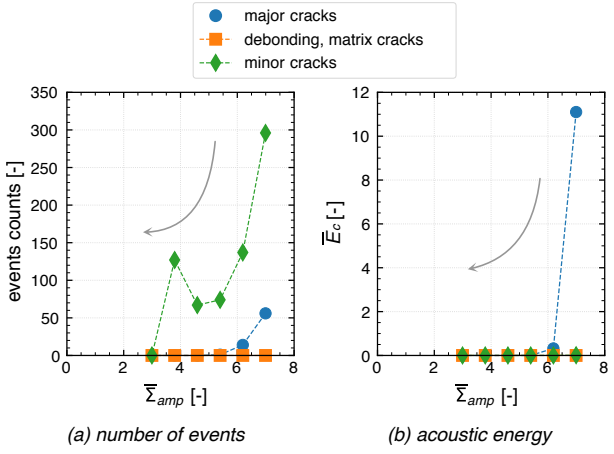

Figure 15. Evolution of the material acoustic activity during a reverse heat build-up test.

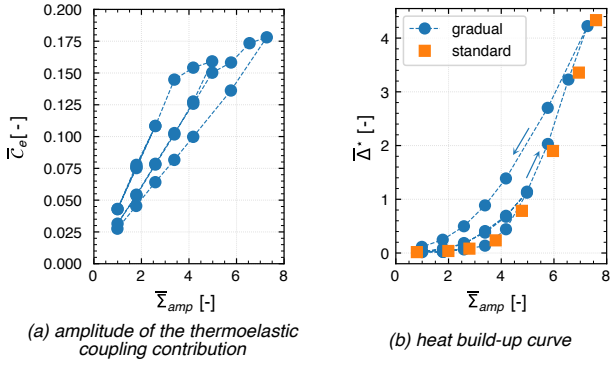

Figure 16. Infrared results of the gradual heat build-up results.

Figure 19 shows the results of the last loading sequence of the gradual heat build-up protocol. Figure 19-(b) reveals the damage progression detected up to the maximum loading step. In this case, the increase in dissipated energy is not uniform and is mostly localised in the upper left corner of the dissipation map, as displayed in Figure 19-(d). This area seems to coincide with the most significant increase in $2 \times f$ amplitudes. Furthermore, when comparing the damage progression in Figure 19-(b) and Figure 18-(b), it is possible to deduce that significant damage development occurred in this highlighted area.

Analysis and discussions

This section summarises the totality of the previously shown results, gives their physical interpretation and proposes a damage and dissipation evolution scenario characteristic to heat build-up experiments performed on this family of materials.

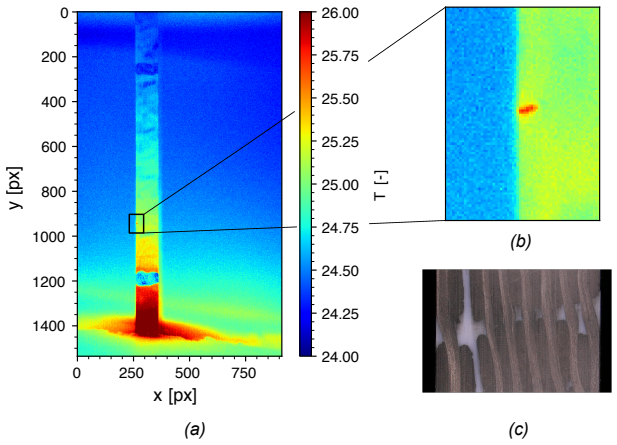

Figure 17. First loading sequence of the gradual heat build-up curve.

Analysis of the experimental data

Heat build-up tests By examining the results obtained using the infrared camera (Figure 10), an increase in the dissipation, which occurs when the stress amplitude exceeds approximately 4 MPa/MPa, becomes apparent. This increase is expressed by an obvious change of slope, as previously observed for this family of materials in [6,39]. This slope change is often referred to as the transition between regime I and regime II and used as an indicator for a fast evaluation of the fatigue lifetime.

Regarding the thermal and the acoustic event detection results (Figures 11 and 13), the first event systematically precedes the aforementioned threshold (4 MPa/MPa). Nevertheless, the total number of these early events and their intensity remain inconsequential. Subsequently, as the stress amplitude applied increases, these events become increasingly frequent and significant in terms of acoustic energy and affected surface. This intensity increases, then seems to saturate for stress amplitudes around 5 to 6 MPa/MPa. These findings agree with the stiffness evolution shown in Figure 12. More specifically, the first stiffness loss was found to correlate with the first peak of the "major crack" class that encompasses the most energetic events, that could lead to a loss of stiffness observable at the scale of the specimen. Once this first peak has been reached, the stiffness continues to decrease until the end of the experiment.

Reverse heat build-up results It was shown that the most significant damage occurs during the first loading step (*i.e.* for the highest stress amplitude), see Figures 14 and 15. This means that, for a given stress amplitude, the damage state is more advanced than in the case of a classic heat build-up test. As the damage state does not progress significantly during the following steps of the reverse heat build-up experiment, it is possible to evaluate the effect of the introduced damage on the value of the dissipated energy. By analysing Figure 14-(a), it becomes immediately apparent that the dissipated energy obtained for a given stress amplitude is higher in the case of the reverse protocol than in the case of a classic heat build-up test. This implies that the formerly introduced damage leads to an increase in dissipation. Moreover, Figure 14-(c) and Figure 14-(d) exhibit a certain correlation between the relative increase in the dissipated energy and the value of $2 \times f$ amplitudes. This would suggest an increased contribution of friction as a dissipation source.

Gradual heat build-up results As shown in Figures 16-(b) and 17, the first loading sequence does not induce any significant damage as the dissipated energy curve does not show any hysteresis and as the thermoelastic coupling remains linear and keeps its initial slope. The hysteresis effect can be observed during the second sequence where the maximum applied stress amplitude reaches 5 MPa/MPa (Figure 18-(a)). This confirms the effect of the introduced damage on the dissipated energy. Since no new cracking occurs after the maximum loading stress has been applied, the increase in dissipated energy observed during the descending steps, must be the result of the previously introduced damage. This damage leads, *inter alia*, to a decrease in the initial slope of the thermoelastic coupling evolution presented in Figure 16-(a). As there is no significant development of friction (that would otherwise be visible in $2 \times f$ amplitude maps displayed in Figure 18-(d) and (e)), this dissipation increase can be related to secondary effects of the previously introduced damage (stress concentration in the vicinity of cracks, micro-friction in the yarns ...). This would also explain why the dissipation increase seems to be concentrated in the areas of the previously detected events (Figure 18). The last

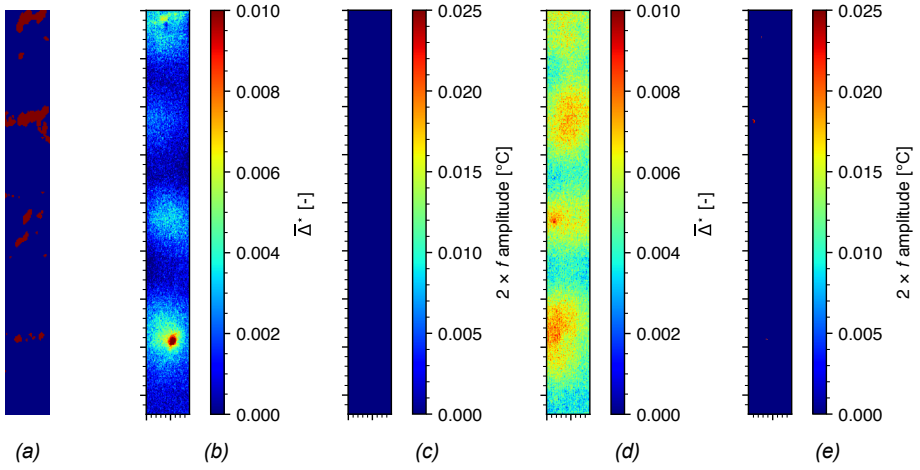

Figure 18. Second loading sequence of the gradual heat build-up curve: (a) location map depicting where thermal events occured during the first block up to normalised stress amplitude $\overline{\Sigma}_{amp} = 5$, (b), resp. (c), dissipation map, resp. $2 \times f$ map, during the first loading for the normalised stress amplitude $\overline{\Sigma}_{amp} = 3.4$ and (d), resp. (e), dissipation map, resp. $2 \times f$ map, during the second loading for the normalised stress amplitude $\overline{\Sigma}_{amp} = 3.4$.

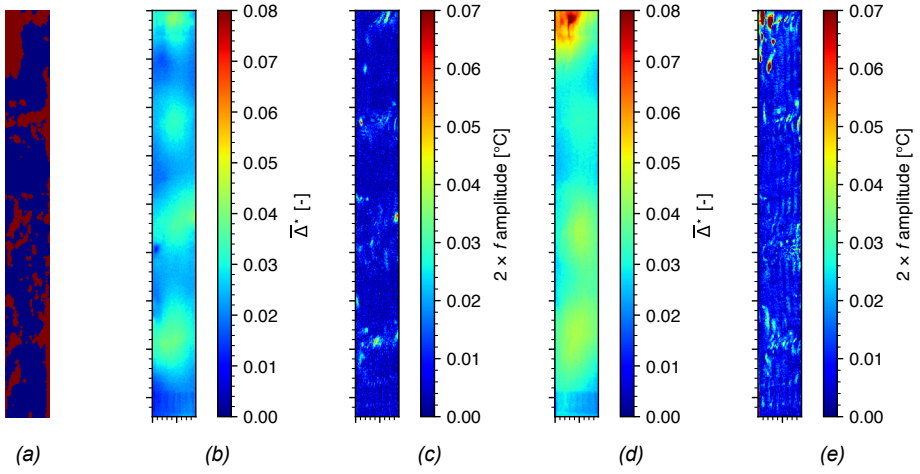

Figure 19. Third loading sequence of the gradual heat build-up curve: (a) location map depicting where thermal events occured during the first block up to normalised stress amplitude $\overline{\Sigma}_{amp} = 7.3$, (b), resp. (c), dissipation map, resp. $2 \times f$ map, during the first loading for the normalised stress amplitude $\overline{\Sigma}_{amp} = 5.8$ and (d), resp. (e), dissipation map, resp. $2 \times f$ map, during the second loading for the normalised stress amplitude $\overline{\Sigma}_{amp} = 5.8$.

sequence illustrates the increasing importance of friction. It shows that the most significant increase in dissipation matches the area highlighted in $2 \times f$ amplitude maps. These results affirm the predominant importance of friction as a dissipation source under relatively high stress levels.

Damage and dissipation scenario of heat build-up experiments

This section proposes a detailed description of the evolution of both damage and different dissipation sources. In the following, the concept of regimes, mentioned in Section *Analysis of the experimental data*, will be adopted. This concept, widely used in studies using thermal measurements to predict the deterministic S-N curve via an energy based criterion [6,14,15,19,39], postulates the existence of several regimes, each regime being related to a specific predominant dissipative mechanism. As mentioned earlier, during a heat build-up experiment, the dissipated energy increases steadily and, then, increases more significantly when the stress amplitude has exceeded the value of

4 MPa/MPa. This value corresponds to the so-called transition between regime I and regime II.

Regime I As illustrated previously, this regime is relatively free of damage as the first cracks occur only at the end of the regime; they are few in numbers and characterised mostly as micro-cracks according to the acoustic emission post-processing results. The dissipated energy and the elastic coupling were shown to be independent of the loading history in this amplitude range and are considered to be the result of the viscoelastic (viscoplastic) behaviour of the epoxy resin (including the resin sealed inside the yarns) as the behaviour of the carbon fibres is assumed to be elastic and therefore non-dissipative.

Regime II The transition between regimes I and II takes place around 4 MPa/MPa of the applied stress amplitude. This regime is characterised by sharp damage growth that hits its peak between 5 to 6 MPa/MPa of the applied stress amplitude and then subsides as the stress continues to increase. The dissipated energy increase is accelerated with respect to regime I. The latter is mostly due to the so-called secondary effects of the cracks induced. These effects were demonstrated throughout the analysis of the second loading sequence of the gradual heat build-up protocol. The associated $2 \times f$ amplitude maps did not indicate any presence of friction.

The results of the reverse heat build-up experiment indicate that the end of this regime might be characterised by a continual increase in friction as a dissipation source. This phenomenon was also highlighted by analysing the results of the last loading sequence of the gradual heat build-up test. This continual increase in friction explains why the dissipated energy continues to grow as the stress amplitude exceeds the value of 7 MPa/MPa, even though the damage state progresses more slowly.

Based upon these results, it is possible to conclude that the heat build-up and the gradual heat build-up protocols are highly interesting for the characterisation of the dissipative mechanisms. The heat build-up test allows the regime transition to be identified. The gradual heat build-up test then enables the effects of the induced damage to be highlighted, thus exposing the role of friction

Conclusions

This article deals with an interlock layer-to-layer woven composite designed for research purposes. The main objective was to identify the dissipative mechanisms activated under cyclic loadings and to describe the evolution of their relative contribution during a heat build-up experiment. This was achieved by coupling the infrared imaging and the acoustic emission monitoring techniques. Apart from dissipation fields evaluated from the infrared data, two specific infrared post-processing methods were applied during this study. The first technique allowed the temperature signature of the cracks occurring under the applied loadings to be located and, hence, allowed the indirect evaluation of the posterior effect of the cracking on the dissipated energy. The second technique allowed those areas exhibiting severe intra-crack friction to be highlighted. The acoustic emission monitoring, employed during the second set of tests, enabled the accurate description of the damage state evolution. This aspect proved to be crucial in the overall understanding of heat build-up curves. The evolution scenario of the dissipated energy was described using the concept of regimes. Two regimes characterised by different dissipative mechanisms were identified. The dissipation evaluated during the first regime was attributed to the non-elastic behaviour of the epoxy resin. The steep increase in dissipation observed during the second regime was mostly due to the secondary effects of the induced damage with a continuous increase in friction contribution. This detailed description of the dissipative mechanisms occurring under cyclic loadings provides an experimental database to constitute modelling comparisons that could pave the way for fatigue life predictions. Yet, these approaches will have to take into account the different effects of the identified mechanisms on fatigue life.

Acknowledgements

The research presented in this article was funded by the Safran Group, France. Safran Tech-Composites Platform is acknowledged for the manufacturing of the samples used in this study. The authors would also like to thank the French ANRT Agency for its financial support (CIFRE n°2017/1456).

A part of this study belongs to the "Self-Heating" ANR - Safran - Naval Group research chair (Grant # ANR-20-CHIN-0002) involving Safran Companies, Naval Group, ENSTA Bretagne (IRDL) and Institut Pprime."

References

1. Naik N, Azad S and Durga Prasad P. Stress and failure analysis of 3d angle interlock woven composites. *Journal of Composite Materials* 2002; 36: 93–123.
2. Tong L, Mouritz A and Bannister M. *3D Fibre Reinforced Polymer Composites*. Elsevier Science, 2002.
3. Nehme S, Hallal A, Fardoun F et al. Numerical/analytical methods to evaluate the mechanical behavior of interlock composites. *Journal of Composite Materials* 2012; 45: 1699–1716.
4. Tableau N, Khellil K, Aboura Z et al. Experimental investigation of the in plane and through thickness shear damages on 3D woven CMC using multi-instrumented torsional tests. In *16th European Conference on Composite Materials (ECCM16)*. Sevilla, Spain.
5. Yu B, Bradley R, Soutis C et al. 2D and 3D imaging of fatigue failure mechanisms of 3D woven composites. *Composites Part A: Applied Science and Manufacturing* 2015; 77: 37–49.
6. Bai G, Lamboul B, Paulmier P et al. Fast fatigue limit estimation of woven composite materials by self-heating analysis. In *12th International Conference on Quantitative Infrared Thermography 2015, (QIRT 2015)*. Mahabalipuram, India.
7. Hurmane A, Mavel A, Paulmier P et al. Combined experimental and modelling approaches for strength analysis of 3d woven composites: from elementary coupons to complex aeronautical structures. *Aerospace Lab* 2016; 12: 1–11.
8. Umer R, Alhussein H, Zhou J et al. The mechanical properties of 3d woven composites. *Journal of Composite Materials* 2017; 51: 1703–1716.
9. Irving P and Soutis C. *Polymer Composites in the Aerospace Industry (second edition)*. Woodhead Publishing, 2019.
10. Jin L, Hu H and Gu B. Three-point bending fatigue behavior of 3d angle-interlock woven composite. *Journal of Composite Materials* 2012; 46: 883–894.
11. Luong M. Fatigue limit evaluation of metals using an infrared thermographic technique. *Mechanics of Materials* 1998; 28: 155–163.
12. Doudard C, Calloch S, Hild F et al. Identification of the scatter in high cycle fatigue from temperature measurements. *Comptes Rendus Mécanique* 2004; 332: 795–801.
13. Munier R, Doudard C, Calloch S et al. Determination of high cycle fatigue properties of a wide range of steel sheet grades from self-heating measurements. *International Journal of Fatigue* 2012; 63: 46–61.
14. Le Saux V, Marco Y, Calloch S et al. Fast evaluation of the fatigue lifetime of rubber-like materials based on a heat build-up protocol and micro-tomography measurements. *International Journal of Fatigue* 2010; 32: 1582–1590.
15. Marco Y, Masquelier I, Le Saux V et al. Fast prediction of the wöhler curve from thermal measurements for a wide range of NR and SBR compounds. *Rubber Chemistry and Technology* 2016; 90: 487–507.
16. Meneghetti G and Quaresimin M. Fatigue strength assessment of a short fiber composite based on the specific heat dissipation. *Composites Part B: Engineering* 2011; 42: 217–225.
17. Jégou L, Marco Y, Le Saux V et al. Fast prediction of the wöhler curve from heat build-up measurements on short fiber reinforced plastic. *International Journal of Fatigue* 2012; 47: 259–267.
18. Serrano L, Marco Y, Le Saux V et al. Fast prediction of the fatigue behavior of short-fiber- reinforced thermoplastics based on heat build-up measurements : application to heterogeneous cases. *Continuum Mechanics and Thermodynamics* 2017; 29: 1113–1133.
19. Leveuf L, Marco Y, Le Saux V et al. Fast screening of the fatigue properties of thermoplastics reinforced with short carbon fibers based on thermal measurements fast screening of the fatigue properties of thermoplastics reinforced with short carbon fibers based on thermal measurements. *Polymer Testing* 2018; 68: 19–26.
20. Karama M. Determination of the fatigue limit of a carbon/epoxy composite using thermographic analysis. *Structure Control & Health Monitoring* 2011; 18: 781–789.
21. Marco Y, Le Saux V, Jégou L et al. Dissipation analysis in SFRP structural samples: Thermomechanical analysis and comparison to numerical simulations. *International Journal*

of Fatigue 2014; 67: 142–150.

22. Ezanno A, Doudard C, Calloch S et al. A new approach to characterizing and modeling the high cycle fatigue properties of cast materials based on self-heating measurements under cyclic loadings. *International Journal of Fatigue* 2013; 47: 232–243.
23. Tsai K, Chiu C and Wu T. Fatigue behavior of 3D multi-layer angle interlock woven composite plates. *Composites Science and Technology* 2000; 60: 241–248.
24. Schneider J. *Mécanismes d'endommagements dans les composites multicouches à renforts interlocks*. PhD Thesis, Université de Technologie de Compiègne, 2011.
25. Henry J. *Etude et analyse des mécanismes d'endommagements en fatigue des composites à renforts tissus interlocks*. PhD Thesis, Université de Technologie de Compiègne, 2013.
26. Jin L, Jin B, Nikhil K et al. Tension-tension fatigue behavior of layer-to-layer 3D angle-interlock woven composites. *Materials Chemistry and Physics* 2013; 140: 183–190.
27. Pankow M, Justusson B, Riosbaas M et al. Effect of fiber architecture on tensile fracture of 3D woven textile composites. *Composite Structures* 2019; 225: 111139.
28. Roget J. émission acoustique. *Techniques de l'Ingénieur* 1990; V3200 V1.
29. Ono K. Trends of recent acoustic emission literature. *Journal of Acoustic Emission* 1990; 12: 177–198.
30. Huguet S. *Application de classificateurs aux données d'émission acoustique : identification de la signature acoustique des mécanismes d'endommagement dans les composites à matrice polymère*. PhD Thesis, INSA Lyon, 2002.
31. Berthelot J. Relation between amplitudes and rupture mechanisms in composite materials. *Journal of Reinforced Plastics and Composites* 1988; 7: 284–299.
32. Barré S and Benzeggagh M. On the use of acoustic emission to investigate damage mechanisms in glass-fibre-reinforced polypropylene. *Composites Science and Technology* 1994; 52: 369–376.
33. Ceysson O, Salvia M and Vincent L. Damage mechanisms characterisation of carbon fibre/epoxy composite laminates by both electrical resistance measurements and acoustic emission analysis. *Scripta Materialia* 1996; 34: 1273–1280.
34. Kim S and Lee Y. Characteristics of damage and fracture process of carbon fiber reinforced plastic under loading-unloading test by using ae method. *Materials Science and Engineering: A* 1997; 234-236: 322–326.
35. Kotsikos G, Evans J, Gibson A et al. Environmentally enhanced fatigue damage in glass fibre reinforced composites characterised by acoustic emission. *Composites Part A: Applied Science and Manufacturing* 2000; 31: 969–977.
36. Marec A, Thomas J and El Guerjouma R. Damage characterization of polymer-based composite materials: Multivariable analysis and wavelet transform for clustering acoustic emission data. *Mechanical Systems and Signal Processing* 2008; 22: 1441–1464.
37. Sisodia S, Gamstedt E, Edgren F et al. Effects of voids on quasi-static and tension fatigue behaviour of carbon-fibre composite laminates. *Journal of Composite Materials* 2015; 49: 2137–2148.
38. Li Z, Guo L, Zhang L et al. In situ experimental investigation on the out-plane damage evolution of 3D woven carbon-fiber reinforced composites. *Composites Science and Technology* 2018; 162: 101–109.
39. Muller L, Roche J, Hurmane A et al. Experimental monitoring of the self-heating properties of thermoplastic composite materials. *Procedia Engineering* 2018; 213: 183–191.
40. Navrátil L. *Apports de l'imagerie qualitative infrarouge pour la caractérisation thermomécanique et le dimensionnement en fatigue de composites tissés 3D*. PhD Thesis, ENSTA Bretagne, 2021.
41. Naderi M, Kahirdeh A and Khonsari MM. Dissipated thermal energy and damage evolution of glass/epoxy using infrared thermography and acoustic emission. *Composites: Part B* 2012; 43: 1613–1620.
42. Tableau N, Aboura Z, Khellil K et al. Multiaxial loading on a 3D woven carbon fiber reinforced plastic composite using tensile-torsion tests: Identification of the first damage envelope and associated damage mechanisms. *Composite Structures* 2019; 227: 111305.
43. Schneider J, Aboura Z, Khellil K et al. Contribution of damage mechanisms comprehension of interlock- reinforced composite materials. In *13th European Conference on Composite Materials (ECCM-13)*. Stockholm.

44. Leveuf L. *Caractérisation et modélisation du comportement mécanique et de la tenue en fatigue d'un composite thermoplastique à fibres de carbone courtes pour applications aéronautiques*. PhD Thesis, ENSTA Bretagne, 2017.
45. Chrysochoos A and Louche H. An infrared image processing to analyse the calorific effects accompanying strain localisation. *International Journal of Engineering Science* 2000; 38: 1759–1788.
46. Meneghetti G. Analysis of the fatigue strength of a stainless steel based on the energy dissipation. *International Journal of Fatigue* 2007; 29: 81–94.
47. Sakagami T, Kubo S, Tamura E et al. Identification of plastic-zone based on double frequency lock-in thermographic temperature measurement. In *11th International Conference on Fracture (ICF11)*. Turin, Italy.
48. Chrysochoos A. Infrared thermography applied to the analysis of material behavior: a brief overview. *Quantitative InfraRed Thermography Journal* 2012; 9: 193–208.
49. Urbanek R and Bär J. Influence of motion compensation on lock-in thermographic investigations of fatigue crack propagation. *Engineering Fracture Mechanics* 2017; 183: 13–25.
50. Mistras. *Digital Signal Processing with AEwin, User's manual*, 2007.